Nanorheology of Adsorbed Diblock Copolymer Layers

Eric Pelletier, Gérald Belder, Georges Hadziioannou, Andrei Subbotin

Nanorheology of Adsorbed Diblock Copolymer Layers

Eric Pelletier ([1]), Gérald F. Belder ([1]), Georges Hadziioannou ([1,*]) and Andrei Subbotin ([2])

([1]) Department of Polymer Chemistry and Materials Science Centre, University of Groningen, Nijenborgh 4, 9747 AG Groningen, The Netherlands
([2]) Institute of Petrochemical Synthesis, Russian Academy of Sciences, Leninski Prospect 29, Moscow 117 912, Russia

(Received 13 May 1996, received in final form 4 October 1996, accepted 7 November 1996)

PACS.81.40.Pq – Friction, lubrication, and wear
PACS.83.50.Fc – Linear viscoelasticity
PACS.83.10.Nn – Polymer dynamics

Abstract. — We investigate the mechanical properties of ultra-thin layers of polystyrene/poly (2-vinylpyridine) (PS/P2VP) block copolymers by means of a Surface Forces Apparatus adapted to operate as a rheometer at the molecular level. Two systems are studied: "brush/wall" and "brush/brush". A comparison of the normal force curves shows that when brushes are compressed against each other, they contract rather than interpenetrate. Nanorheological experiments have been carried out on both systems but reliable measurements have been obtained only on the brush/wall system. The complex shear modulus, characterizing the confined medium, has been measured as a function of separation. Its distance dependence is compared with a scaling model describing the linear shear behaviour of a brush confined by a neutral surface.

1. Introduction

Polymer chains adsorbed or grafted onto a solid surface have been widely studied because of their technological interest as surface modifiers [1]. In recent years, the Surface Forces Apparatus has been employed to measure the quasi-equilibrium force-distance profile between surfaces bearing adsorbed or grafted layers [2]. Such a profile can be directly compared with theoretical models describing molecular interactions between polymer layers.

Much less work has been performed on the rheological properties of adsorbed layers. Knowledge of such properties is important since polymeric interfaces are involved in a large variety of phenomena such as adhesion, friction and fracture of soft materials [3]. One of the best ways to get direct insight in their viscoelastic properties is to use a Surface Forces Apparatus adapted to operate as a rheometer [4]. Only very few results have been published about the linear viscoelastic properties of such layers. Two kinds of motions have been used to measure the complex shear modulus characterizing the linear viscoelasticity of ultra-thin films confined between solid surfaces. Normal periodic oscillations were employed to measure the complex modulus describing the viscoelastic behaviour of adsorbed layers [5, 6]. However, as the layers were compressed, the storage shear modulus was progressively hidden by the normal force

(*) Author for correspondence (e-mail: hadzii@rugch5.chem.rug.nl)

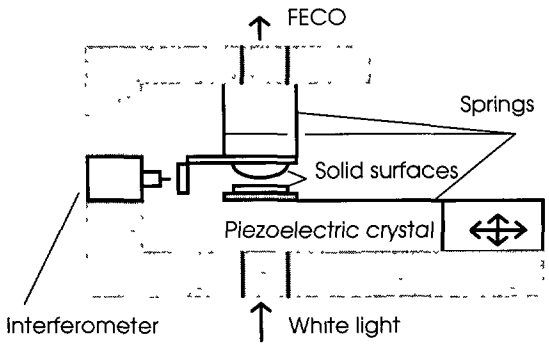

Fig. 1. — Scheme of the apparatus.

due to the confinement of the layers. Tangential oscillations performed on ultra-thin layers of polymer melt have also been employed [7–9] to measure the linear shear modulus and study its variation with the confinement.

In this paper, we focus on the properties of diblock copolymer layers adsorbed onto mica from a selective solvent. Such layers have been the subject of numerous studies [10–14] and can be favourably compared with brushes. In the first part, we study the normal static force profile between a mica surface bearing a brush and a bare mica surface. The emphasis is put on a comparison with the force profile between two brushes, obtained from the same sample, to verify the non-interpenetration assumption which is usually made. The second part is devoted to oscillatory shear experiments on a brush/wall system. We present the variation of the linear shear modulus with confinement. These results are compared with a scaling model describing the shearing of a brush/wall system in a linear regime of deformation.

2. Experimental Section

2.1. Apparatus. — We will only give a brief description of the apparatus (Fig. 1) since a complete description will be published elsewhere [15]. The apparatus is based on the design by Israelachvili [16]. However, some modifications have been implemented to allow the measurement of both normal and tangential forces at the same time. The lower surface is mounted at the end of a horizontal leaf spring which is classically used to measure normal forces. The upper surface is suspended from two vertical leaf springs whose deflection is measured by means of a very sensitive two-beam fibre interferometer [17]. The tangential force then follows from the known stiffness of the leaf springs. The force resolution for normal and tangential forces is close to 10^{-7} N. The liquid cell, to which the end of the horizontal spring is connected, is moved by means of an XY piezoelectric block. This system allows a very fine control of both normal and tangential displacements. During shear measurements, the lower surface is set in controlled lateral motion, $X_1(t)$, while the resulting motion of the upper surface, $X_2(t)$, is measured. The strain within the gap, $\epsilon = (X_1 - X_2)/D$ — D is the solid surfaces separation — cannot be imposed since it depends both on the leaf springs stiffness and on the properties of the medium. In order to measure the viscoelastic properties of the confined medium, a sinusoidal motion is imposed to the lower surface: $X_1(t) = X_1^0 \sin(\omega t)$. The motion of the upper surface, $X_2(t) = X_2^0 \sin(\omega t + \varphi)$, is followed with an oscilloscope while the amplitude of the motion X_2^0 and the phase shift φ are measured by means of a lock-in amplifier. From these data and the surface separation D, which is classically measured by the FECO technique, the complex shear

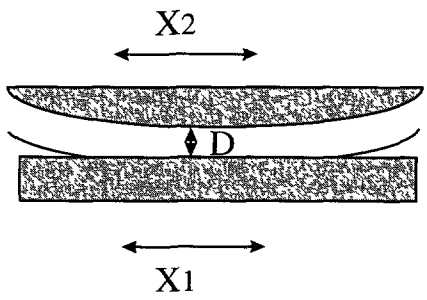

Fig. 2. — Magnification of the interfacial area. A layer is confined by two solid surfaces. D is the smallest separation between the solid surfaces. X_1 and X_2 are the displacement of the lower and the upper surfaces, respectively.

modulus G^* is calculated. It should be noted that the measurements are performed between curved surfaces. The sheared area is defined by the flattened contact area of the layers which give the main contribution to the tangential force (Fig. 2). In addition, the surface separation ($\sim$ 20 nm) is negligible in comparison with the radius of curvature of the surfaces ($\sim$ 1 cm) and justifies the approximation of simple shear in the case of a displacement comparable with D.

2.2. SAMPLES. — Freshly cleaved muscovite ruby-red mica (grade 4 ASTM V-2 clear and slightly stained) is used as the substrate surface for the experiments.

The polystyrene/poly(2-vinylpyridine) (PS/P2VP) block copolymer employed has the following characteristics: weight-averaged molecular weight: $M_{\mathrm{wP2VP}} = 3\ 400$ g mol^{-1}, $M_{\mathrm{wPS}} = 75\ 000$ g mol^{-1} and polydispersity index $P = 1.04$. Analytical grade toluene from Merck is used as a solvent. The experiments are performed at a constant temperature of 21.0 ± 0.5 °C.

The toluene solvates the PS blocks but not the P2VP ones. The unperturbated radius of gyration of the PS block is estimated to be $R_{\mathrm{g}} = 1.86\ M_{\mathrm{w}}^{0.585} = 95$ Å [18].

When the solution is in contact with the mica surfaces, the P2VP block adsorbs and anchors the PS block to the surface [10]. PS is known not to adsorb onto mica from toluene [19]. The repulsive interactions between the PS segments stretch the PS blocks far away from the surface, creating relatively thick layers. In addition, the small size of the P2VP allows the comparison of such layers to real brushes.

2.3. PROCEDURE. — Thin sheets of back-silvered mica are glued onto the lenses. The glue is a mixture 50/50 by weight of dextrose and galactose. The apparatus is flushed with argon for half an hour prior to the experiment. The contact position is defined by the adhesive contact between the surfaces in argon. All distances between the mica surfaces refer to this contact point.

Surface forces are first recorded in pure solvent to check for the absence of contamination. Then, 1 ml of diblock copolymer solution is added to the liquid cell containing 10 ml of solvent, leading to a final concentration of 5×10^{-5} g ml^{-1} This concentration is lower than the critical micelle concentration: 6×10^{-5} g ml^{-1}, obtained by integral light scattering on similar systems [20]. The surfaces are kept well-separated (at around 1 mm) in order to allow the polymer to diffuse throughout the liquid cell. After a sufficient time for the adsorbed layers to reach equilibrium, the force profile between the surfaces is measured. This procedure applies to the measurement of the force profile between two brushes. Some modifications are needed to study the brush/wall system. After measuring the contact in pure toluene, the upper surface

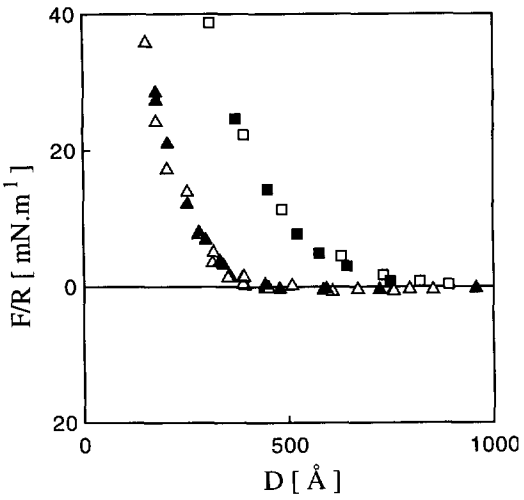

Fig. 3. — Plot of F/R as a function of the surface separation D for the brush/wall system (△) and the brush/brush system (□). Filled symbols are for compression while the empty symbols indicate decompression.

is taken out and 1 ml of solution containing the diblock copolymer is added to the toluene. Following an incubation time of 24 h, the solution is replaced by pure toluene and the upper surface is put back into place. Then, the force profile is measured as usual.

The shear experiments are performed as a function of the separation between the mica surfaces. The normal displacement of the piezoelectric block, used to adjust the separation, is stopped and the system is allowed to relax. This time is usually a few minutes and the relaxation is followed by observing the fringes displacement. After the cessation of all detectable relaxation, shear measurements are performed and both normal and tangential forces are measured. This procedure is repeated several times at different distances during a force run to obtain a good insight into the properties of the confined medium.

3. Static Interactions

3.1. RESULTS. — The compression of the diblock polymer layers (Fig. 3) results in a monotonous repulsive force with a range reflecting the extension of the PS blocks far away from the surfaces (~ 900 Å). When the force profile of the brush/wall system is measured, only repulsion is detected. In addition, the range of the force profile (~ 450 Å) is reduced by a factor of two in comparison with the brush/brush system. In order to make a closer quantitative comparison, the distance D used to define the force profile of the brush/wall system is multiplied by a factor of two. The resulting force curve, shown in Figure 4, proves that a good correlation exists between the measurements performed on both systems.

3.2. DISCUSSION. — The interactions between adsorbed diblock copolymer layers have received considerable attention [21]. The repulsion between such layers has been analysed with different models [22–24]. The physics is commonly analysed [22] in terms of the sum of an osmotic repulsive force, increasing with the brush confinement, and an elastic restoring force which decreases as the chains become less stretched. It is also assumed that when the layers are compressed against each other, they contract rather than interpenetrate. In this case,

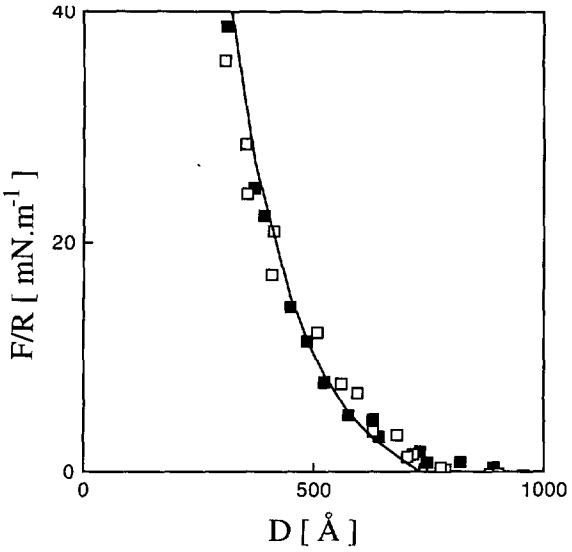

Fig. 4. — Superposition of F/R as a function of D for the brush/brush system (■) and the brush/wall (□) system. The abscissa values for the brush/wall system have been scaled by a factor of 2. The full line represents the theoretical fit following [21].

the force profile of a single layer against a bare surface, without specific interaction, is expected to be the same as the force profile of two layers compressed against each other.

In the case of a layer of PS/P2VP in toluene compressed against a mica surface, no bridging is expected as the non-adsorbance of PS from toluene onto mica has been shown [19]. Hence, the hypothesis of non-interpenetration between the layers can be directly checked by a comparison between the force profiles for PS/mica and PS/PS.

Such a comparison has already been performed on a similar system — PS/PEO in toluene — with PS segments of higher molecular weight [25]. However, only qualitative comparisons concerning the shape of the force curves and the range of the brush/wall interaction were made.

In Figure 4, the PS/mica force profile has been scaled by a factor of 2 to compare it with the brush/brush system. The correlation between the force profiles is very good since the two curves perfectly overlap.

The interpenetration between juxtaposed layers has been numerically studied [11, 26]. The authors show that the interpenetration can be important, depending on the confinement level of the layers, but that it does not strongly affect the force profile. The measurements have been performed on moderately confined layers since the onset of detectable forces is around 900 Å and the layers have been compressed to a thickness of approximately 300 Å. Over this range, the interpenetration does not seem to affect the normal force response.

These results show that the force profile is quite insensitive to the interpenetration which could occur between the layers according to the theoretical models already mentioned [11, 26]. Thus, the force profiles can be fitted using models assuming non-interpenetration between the layers such as the model by Milner, Witten and Cates (MWC) [23]. This allows an estimation of the adsorbance by following the procedure described in [21]. The MWC model is used to fit the force-distance curve within a numerical factor. This numerical factor is assumed to characterize the system PS/toluene and is determinated by complementary measurements. Using the factor determined by Patel and Tirrell [21], we found the adsorbance $\Gamma \cong 3$ mg m^{-2} *This value*

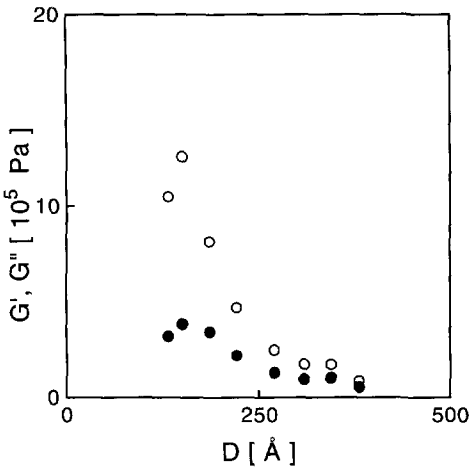

Fig. 5. — Storage G' (○) and loss G'' (●) modulus as a function of D.

corresponds to an average separation between "anchor points" of $d = 2(M_{wPS}/(\pi N_0 \Gamma))^{1/3} \cong$ 73 Å, where N_0 is Avogadro's constant. This value is lower than the PS unperturbed radius of gyration, 95 Å. It shows, together with the layer thickness $\sim$ 450 Å, that the chains are stretched within the brush.

The weak interpenetration between juxtaposed brushes is also supported by shear experiments. Even by compressing the layers up to half their equilibrium thickness, we have not been able to measure appreciable tangential forces. We have applied only small deformations, such that the strain was kept lower than 1, at relatively low frequencies. Hence, these measurements cannot be compared to those described in [27] where brushes were sheared past each other at very high amplitude and high frequencies. However, the results support each other since both show that brushes sliding past each other display very weak friction coefficients.

4. Shear Measurements

4.1. Results. — Shear measurements have been performed between a bare mica surface and a brush. Figure 5 shows the storage modulus, G', and the loss modulus, G'', as a function of the closest separation D between the mica surfaces. The measurements have been carried out at a constant frequency of 10 Hz and a strain lower than unity. The shearing has been performed at distances below the first contact between the adsorbed layer and the mica surface. At distances beyond the threshold of the static force, we have not been able to measure any tangential forces. The flattened surface of the layer has been defined as the sheared area since the tangential forces arising from the curved edges can be neglected. Figure 5 shows that both G' and G'' increase as the separation is decreased and that G' is larger than G'' at all measured distances. Hence, the viscoelastic behaviour is dominated by the elastic component.

In order to check for any influence of the tangential displacement on the structure of the layer, the normal force is also measured during the shear experiment. The resulting force profile is compared with the force profile measured before the shear displacements (Fig. 6). It shows no distinguishable change. This indicates that the layer structure is not altered by the tangential displacement of the surfaces.

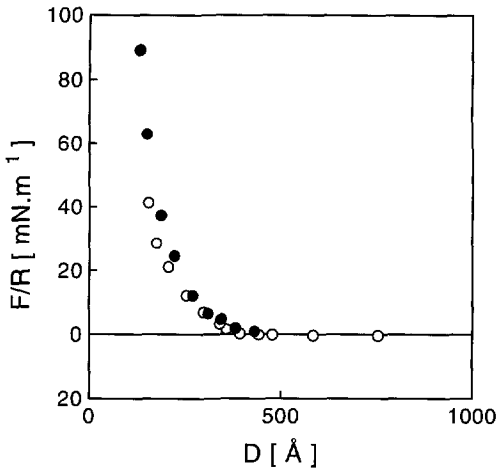

Fig. 6. — Plot of F/R as a function of D: before (○) and during shearing (●).

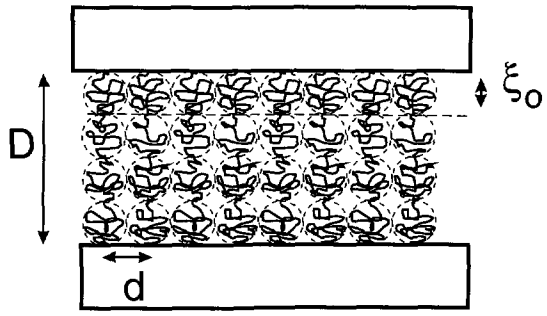

Fig. 7. — Scheme of the sheared brush. D is the separation between the solid surfaces, ξ_0 is the mesh size of the polymer layer and d is the distance between anchor points.

4.2. THEORETICAL MODEL. — We discuss the case of a brush confined between flat surfaces as described in Figure 7. D denotes the surface separation while D_c is the uncompressed equilibrium brush thickness. It is assumed that there are no specific interactions between the brush and the upper surface. The equilibrium properties of a semi-dilute brush are presented in the first part, which introduces the characteristic parameters needed to derive the complex shear modulus.

We consider a dense brush on a solid surface with an average distance between anchor points, d, much lower than the Flory radius of the chain. A step-like concentration profile of the brush is assumed. The average concentration Φ within the brush is:

$$\Phi \approx \frac{N}{Dd^2} \tag{1}$$

where N is the number of segments of one chain. However, the concentration is also connected

to the mesh size ξ_0 [28] by the relation:

$$\Phi \approx \frac{g_0}{\xi_0^3} \approx a^{-3} \left(\frac{\xi_0}{a}\right)^{\frac{1}{\upsilon}-3} \tag{2}$$

$g_0 \approx a^{-1}\xi_0^{1/\upsilon}$ is the number of segments within a mesh and υ is the Flory exponent ($\upsilon = 3/5$ for a good solvent).

Thus, it is possible to directly express ξ_0 as a function of D by combining equation (1) and equation (2):

$$\xi_0(D) \approx a \left(\frac{Dd^2}{Na^3}\right)^{\frac{\upsilon}{3\upsilon-1}} \tag{3}$$

Numerical applications in case of a good solvent lead to $\xi_0 \propto D^{3/4}$.

In the case of shearing a brush against a solid surface, we can consider the brush as a non-homogeneous network with entanglements. The elastic modulus of this network is determined both by the entanglements and by the stretching of the chains [29]. First, we derive the elastic modulus E_1 induced by the entanglements.

In order to estimate the modulus E_1, let us introduce the average number, N_e, of concentration blobs of size ξ_b between the entanglements, — N_e does not change with the concentration. In addition, ξ_b and ξ_0 scale in the same way with Φ. E_1 is thus expressed as:

$$E_1 \sim \frac{k_b T}{\xi_0^3 N_e} \sim \frac{k_b T}{a^2 N_e} \left(\frac{Na^3}{Dd^2}\right)^{\frac{3\upsilon}{3\upsilon-1}} \tag{4}$$

E_1 varies as $D^{-9/4}$ in good solvent.

The second contribution to be taken into account is the stretching of the chains. The average stretching force f_n of a chain within the brush is:

$$f_n \approx \frac{k_b T D}{\xi_0^2 (N/g_0)} \sim \frac{D k_b T}{a^2 N} \left(\frac{\xi_0}{a}\right)^{\frac{1}{\upsilon}-2} \tag{5}$$

The maximum stretching force corresponds to the situation $D \sim D_c$, where D_c is the equilibrium thickness of the brush. In this case $\xi_0 \sim d$.

When submitted to a small shear strain ϵ, the chain is stretched in the tangential direction by the force $f_t \sim f_n \epsilon$. Hence, σ, the shear stress, can be expressed as:

$$\sigma \sim \frac{f_t}{d^2} \sim \frac{1}{d^2} f_n \epsilon. \tag{6}$$

The elastic modulus accounting for the stretching of the chains is thus directly deduced:

$$E_2 \sim \frac{f_n}{d^2} \sim \frac{D k_b T}{a^2 N d} \left(\frac{\xi_0}{a}\right)^{\frac{1}{\upsilon}-2} \sim \frac{D k_b T}{a^2 N d^2} \left(\frac{Dd^2}{Na^3}\right)^{\frac{1-2\upsilon}{3\upsilon-1}} \tag{7}$$

In the case of good solvent conditions, E_2 varies as $D^{3/4}$

It has to be noticed that the variations of E_1 and E_2 are opposed. E_2 will dominate for weak compression, when the chains are still stretched within the brush, while E_1 dominates at

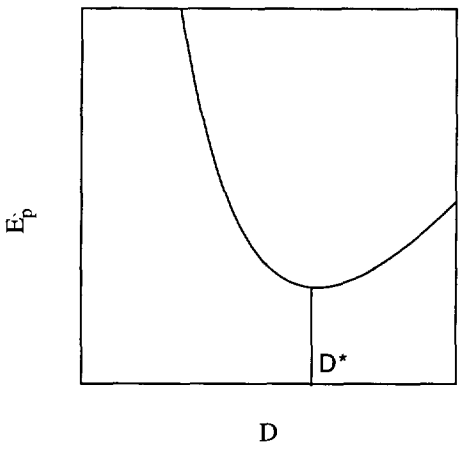

Fig. 8. — Schematic variation of the elastic modulus E_p as a function of D. D^* denotes the distance at which E_p is minimum.

a higher compression level. The distance D^* where the difference of behaviour occurs can be estimated by minimizing the total elastic modulus, $E_p = E_1 + E_2$, with respect to D (Fig. 8).

This leads to the relationship:

$$D^* \propto N_e^{\frac{1-3\upsilon}{4\upsilon}} D_c \tag{8}$$

where $D_c \sim aN\left(\frac{d}{a}\right)^{1-\frac{1}{\upsilon}}$ D_c is determined from equation (1) with $\xi_0 = d$. Numerical application with $\upsilon = 3/5$ gives $D^* \propto N_e^{-1/3} D_c$.

We restrict our analysis to the case $E_1 \gg E_2$ and thus to $D < D^*$ since this regime should dominate for confined layers.

Considering tangential flow at the surface of the brush and using the analogy with semidilute solutions and continuous stress requirements, we can conclude that the flow penetrates only over a thickness ξ_0 into the confined brush [30, 31]. This thickness defines what is called the hydrodynamic penetration layer.

The hydrodynamic layer is the ξ_0 layer in contact with the wall. Hence, all the friction takes place in this layer. The apparent viscosity of the polymer network η_p can be defined as:

$$\eta_p \sim \eta_s \frac{D}{\xi_0} \propto D^{\frac{1-2\upsilon}{1-3\upsilon}} \tag{9}$$

where η_s is the solvent viscosity.

The relaxation time of the polymer network, τ_p, is estimated from the relationship:

$$\tau_p \sim \frac{\eta_p}{E_p} \sim \frac{\eta_s}{k_b T} N_e \xi_0^2 D \propto D^{\frac{5\upsilon-1}{3\upsilon-1}} \tag{10}$$

The next step is to calculate the modulus accounting for the polymer network contribution.

Different cases have to be considered according to the value of $\tau_p\omega - \omega$ is the frequency of the applied strain [31].

If $\tau_p\omega \ll 1$, the behaviour is liquid-like and we can write the following relations:

$$\begin{cases} G''_p & \sim & \eta_p\omega \\ G'_p & \sim & (\omega\tau_p)G''_p \end{cases} \tag{11}$$

G'_p and G''_p are the in-phase and the out-of-phase components of G^*_p, respectively.

The substitution of (10) into (11) yields an expression of G'_p as a function of E_p:

$$G'_p \sim E_p(\omega\tau_p)^2. \tag{12}$$

It has to be noted that in this regime $G'_p \ll G''_p$.

In case of $\tau_p\omega \gg 1$, the chains of the network do not have the time to relax and the behaviour is rubber-like. The polymer network contribution to the shear modulus, G^*_p, can be written as:

$$G'_p \sim E_p \quad \text{and} \quad G''_p \sim (\omega\tau^*_p)^{-1}E_p. \tag{13}$$

Equation (13) shows that G'_p dominates G''_p. In order to derive the global shear modulus, the solvent contribution, G^*_s, to the shear modulus has to be considered. With the assumption of a Newtonian solvent, G^*_s is defined as:

$$G'_s = 0 \quad \text{and} \quad G''_s \sim \omega\eta_s\frac{D}{\xi_0} \tag{14}$$

The components of the total modulus G^* can thus be written as:

$$\begin{cases} G' & = & G'_p + G'_s = G'_p \sim E_p \\ G'' & = & G''_p + G''_s \sim G''_p + \eta_s\omega\dfrac{D}{\xi_0} \end{cases} \tag{15}$$

Usually, the solvent contribution to the global modulus can be neglected in comparison with the polymer one, leading to the relationship:

$$\tau_p\omega \ll 1 \quad \begin{cases} G' & \sim & \dfrac{\omega^2\eta_s^2 aN_e}{k_bT}D^2\left(\dfrac{Dd^2}{Na^3}\right)^{\frac{\upsilon}{3\upsilon-1}} \\ G'' & \sim & \dfrac{\omega\eta_s}{a}D\left(\dfrac{Dd^2}{Na^3}\right)^{\frac{\upsilon}{1-3\upsilon}} \end{cases}, \tag{16}$$

$$\tau_p\omega \gg 1 \begin{cases} G' & \sim & \dfrac{k_bT}{a^3N_e}\left(\dfrac{Na^3}{Dd^2}\right)^{\frac{3\upsilon}{3\upsilon-1}} \\ G'' & \sim & \dfrac{1}{a\eta_sD\omega}\left(\dfrac{k_bT}{a^3N_e}\right)^2\left(\dfrac{Na^3}{Dd^2}\right)^{\frac{5\upsilon}{3\upsilon-1}} \end{cases} \tag{17}$$

Numerical applications for the good solvent case and $D < D^*$ lead to the scaling laws:

$$\tau_p\omega \ll 1 \begin{cases} G' & \propto & D^{11/4} \\ G'' & \propto & D^{1/4} \end{cases}, \tag{18}$$

$$\tau_p\omega \gg 1 \begin{cases} G' & \propto & D^{-9/4} \\ G'' & \propto & D^{-19/4} \end{cases}. \tag{19}$$

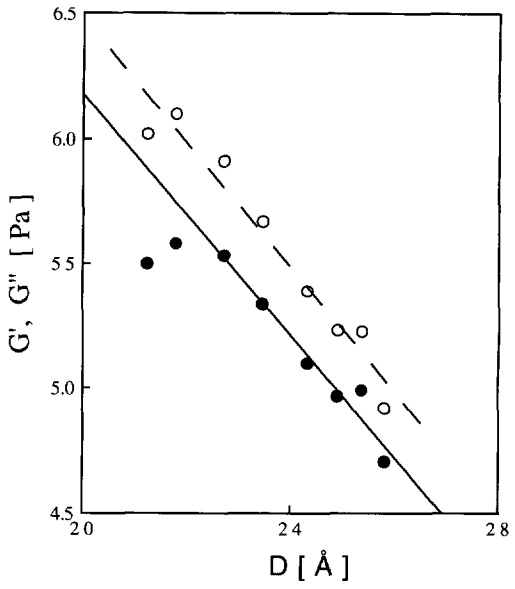

Fig. 9. — Plot of G' (○) and G'' (●) as a function of D in a log-log representation. The straight lines represent the linear fitting by a root-mean-square method. The points obtained for the closest separations have not been taken into account in the fitting.

4.3. DISCUSSION. — The normal force measurements performed during the shear experiments show that no changes occur with respect to the situation before shear (Fig. 6). Hence, the shear process does not cause noticeable changes to the layer structure. It is also shown that the normal force component which should appear during the tangential displacement of the curved surfaces [32] is lower than the force resolution of the apparatus. This supports the approximation of pure shear within the flattened area of the layer since, in addition, $D/R < 10^{-5}$

The determination of a finite shear modulus for the brush/wall system is quite surprising since it was impossible in the case of the brush/brush system. It is well-known that the interactions PS/mica are very weak in toluene. Such interactions should lead to extremely weak friction. However, reliable data have been obtained for confined layers ($D < D_c$) showing that the normal force which compresses the layer compensate for this effect.

The variation of the shear modulus in Figure 5 shows the dominant role of the storage modulus G' as the layer is confined. The values obtained for $G' \sim 10^5 - 10^6$ Pa are in the range expected for a rubbery plateau modulus. In addition, the mean concentration Φ^* of the confined brush is well within a semidilute regime, $\Phi^* \sim \Gamma/D_c = 60$ mg ml^{-1}, since the overlap concentration of the PS segments is estimated to be $(M_{wPS}/N_0)/(4/3\pi R^3_{gPS}) = 34$ mg ml^{-1}. The variations of the shear moduli are connected to the hydrodynamic layer thickness as explained in the theoretical part.

Equation (19) applies to describe the viscoelastic behavior as a function of the separation for $\tau_p\omega \gg 1$. We assume that this relation can be applied to our case since the storage modulus is in the range expected for a rubery plateau and the model qualitatively describes the monotonous increase of G' and G'', with G' dominating G''. Thus, by using equation (19) we assume that $\tau_p \gg 1/2\pi\upsilon \cong 1.6 \times 10^{-2}$ s. A comparison with the experimental data is performed in Figure 9. The linear variation of G' and G'' as a function of D, in a log-log representation, shows that

$G'(D)$ and $G''(D)$ can be described by a scaling law. A root-mean-square adjustment gives the exponents -2.49 and -2.42 for G' and G'', respectively. The comparison with the theoretical predictions shows a good agreement for G', the theoretical prediction is -2.25, and a very poor one for G'', the theoretical prediction beeing -4.75. The factors that explain these discrepancies are various. The solvent quality may change with the concentration. It is well-known that the Flory coefficient varies with the concentration. However, we suggest another explanation. The main assumption of the model is that the solvent viscosity is constant within the gap. In fact, the solvent viscosity should increase near the wall. At some critical distance z^* from the wall, the viscosity starts to increase. Its variations affect the hydrodynamic layer which is located close to the wall. We assume a scaling dependence of $\eta_s(z)$:

$$\eta_s(z) \propto z^{-y} \tag{20}$$

where y is a constant and z is the distance to the wall.

Hence, across the hydrodynamic layer of thickness ξ_0 — within the assumption $z^* > \xi_0$ — we can define an average solvent viscosity $\overline{\eta}_s \propto \xi_0^{-y}$ $\overline{\eta}_s$ has to replace the constant solvent viscosity η_s used in the equations presented in the theoretical part. $\xi_0(D)$ is known from equation (3). Hence, the equation (17) leads to $G''(D)$:

$$G'' \propto D^{\frac{\upsilon(y-5)}{3\upsilon-1}} D^{-1} \tag{21}$$

A simple application, with the assumption that the good solvent parameter υ is still valid, gives $G'' \propto D^{(3y-4)/4}$. A comparison with the exponent derived from the experimental data, -2.42, furnishes $y \sim 3.1$. Direct measurements to verify the validity of this exponent have not been yet performed. However, it has to be noticed that the dynamic behaviour of polymer chains at surfaces can furnish an indirect measurement of the solvent properties close to a solid wall.

5. Conclusion

We have studied the mechanical properties of PS/P2VP layers adsorbed onto mica from toluene. Normal force and shear measurements have both been performed.

Normal force measurements have been carried out on two kinds of systems, brush/wall and brush/brush, to verify the hypothesis of non-interpenetration between brushes. The system studied showed no noticeable interpenetration effect affecting the normal force. The results of shear measurements on the brush/brush system support this conclusion since we have not been able to detect tangential forces.

In contrast, the shear measurements performed on the brush/wall system have been successful, despite the lack of affinity of PS segments for mica in the presence of toluene. A theoretical model has been formulated that describes the variation of the shear modulus with confinement in the linear regime. A comparison with the experimental shear modulus showed a good agreement for the storage modulus but some discrepancies remained to be solved in order to explain the variations of $G''(D)$. The introduction of the solvent viscosity variation close to the surface allows to solve this problem. In addition, it shows that indirect informations about the solvent properties close to solid surfaces can be obtained from the behaviour of polymer chains.

Experiments are currently in progress to check for the variations of the shear modulus with frequency and adsorbance. These measurements will allow a more complete comparison with the model presented since a determination of the polymer network relaxation time should be possible.

Acknowledgments

We thank Paul van Hutten for its careful reading of this manuscript. This research was supported by the Netherlands Foundation of Technology (STW) and the Human Capital and Mobility Network of "Functional Materials Organized at the Supramolecular Level".

References

[1] Faraday discussions "Polymers at surfaces and interfaces " 98 (1995).
[2] Israelachvili J.N., Intermolecular and Surface Forces (Academic Press, London, 1985).
[3] de Gennes P.G., Simple views on condensed matter (World Scientific Publishing Co. Pte. Ltd., Singapore, 1992).
[4] Pelletier E., Montfort J.P. and Lapique F., *J. Rheol.* **38** (1994) 1151.
[5] Pelletier E., Montfort J.P., Loubet J.L., Millot S., Tonck A. and Georges J.M., "Theoretical and Applied Rheology", P. Moldenaers and R. Keunings, Eds., Proc. X^{ith} Int. Congr. on Rheology, Brussels (1992) p. 489.
[6] Pelletier E., Montfort J.P., Loubet J.L., Tonck A. and Georges J.M., *Macromolecules* **28** (1995) 1990.
[7] Granick S. and Hu W., *Langmuir* **10** (1994) 3857.
[8] Peanasky J., Cai L.L. and Granick S., *Langmuir* **10** (1994) 3874.
[9] Hu W. and Granick S., *Science* **258** (1992) 1339.
[10] Hadziioannou G., Patel S., Granick S. and Tirrell M., *J. Am. Chem. Soc.* **108** (1986) 2869.
[11] Whitmore M.D. and Noolandi J., *Macromolecules* **23** (1990) 3321.
[12] Marques C.M., Joanny J.F. and Leibler L., *Macromolecules* **21** (1988) 1051.
[13] Field J.B., Toprakcioglu C., Dai L., Hadziioannou G., Smith G. and Hamilton W., *J. Phys. II France* **2** (1992) 2221.
[14] Patel S., Tirrell M. and Hadziioannou G., *Coll. Surf.* **31** (1988) 157.
[15] Belder G., Pelletier E., Stamouli A. and Hadziioannou G, in preparation.
[16] Israelachvili J.N. and Adams G.E., *J. Chem. Soc. Faraday Trans. I* **74** (1978) 975.
[17] Rugar D., Mamin H.J. and Güthner P., *Appl. Phys. Lett.* **55** (1989) 2588.
[18] Higo Y., Ueno N. and Noda I., *Polymer J.* **15** (1983) 367.
[19] Luckham P.F. and Klein J., *Macromolecules* **18** (1985) 721.
[20] Tang W.T., PhD Thesis, Stanford University (1987).
[21] Patel S. and Tirrell M., *Ann. Rev. Phys. Chem.* **40** (1989) 597.
[22] de Gennes P.G., *Adv. Coll. Interf. Sci.* **27** (1987) 189.
[23] Milner S.T., Witten T.A. and Cates M.E., *Macromolecules* **21** (1988) 2610.
[24] Semenov A.N., Joanny J.F. and Khokhlov A.R., *Macromolecules* **28** (1995) 1066.
[25] Taunton H.J., Toprakcioglu C., Fetters L.J. and Klein J., *Macromolecules* **23** (1990) 571.
[26] Martin J.I. and Wang Z.G., *J. Phys. Chem.* **99** (1995) 2833.
[27] Klein J., Perahia D., Warburg S. and Fetters L.J., *Nature* **352** (1991) 143.
[28] de Gennes P.G., Scaling concepts in polymer physics (Cornell University Press, Ithaca, 1979).
[29] Semenov A.N., *Langmuir* **11** (1995) 3560.
[30] Fredrickson G.H. and Pincus P., *Langmuir* **7** (1991) 786.
[31] Doi M. and Edwards S.F., The theory of polymer dynamics (Oxford Sci. Publ., Oxford, 1986).
[32] Sekimoto K. and Leibler L., *Europhys. Lett.* **23** (1993) 113.